Translational Oncology
www.transonc.com

Volume 7 Number 6 December 2014 pp. 759–767 759

Noninvasive Characterization of Locally Advanced Breast Cancer Using Textural Analysis of Quantitative Ultrasound Parametric Images

Hadi Tadayyon*,†, Ali Sadeghi-Naini*,†,‡,§ and Gregory J. Czarnota*,†,‡,§

*Physical Sciences, Sunnybrook Research Institute, Sunnybrook Health Sciences Centre, Toronto, ON, Canada; †Department of Medical Biophysics, Faculty of Medicine, University of Toronto, Toronto, ON, Canada; ‡Department of Radiation Oncology, Odette Cancer Centre, Sunnybrook Health Sciences Centre, Toronto, ON, Canada; §Department of Radiation Oncology, Faculty of Medicine, University of Toronto, Toronto, ON, Canada

Abstract

PURPOSE: The identification of tumor pathologic characteristics is an important part of breast cancer diagnosis, prognosis, and treatment planning but currently requires biopsy as its standard. Here, we investigated a noninvasive quantitative ultrasound method for the characterization of breast tumors in terms of their histologic grade, which can be used with clinical diagnostic ultrasound data. *METHODS:* Tumors of 57 locally advanced breast cancer patients were analyzed as part of this study. Seven quantitative ultrasound parameters were determined from each tumor region from the radiofrequency data, including mid-band fit, spectral slope, 0-MHz intercept, scatterer spacing, attenuation coefficient estimate, average scatterer diameter, and average acoustic concentration. Parametric maps were generated corresponding to the region of interest, from which four textural features, including contrast, energy, homogeneity, and correlation, were determined as further tumor characterization parameters. Data were examined on the basis of tumor subtypes based on histologic grade (grade I versus grade II to III). *RESULTS:* Linear discriminant analysis of the means of the parametric maps resulted in classification accuracy of 79%. On the other hand, the linear combination of the texture features of the parametric maps resulted in classification accuracy of 82%. Finally, when both the means and textures of the parametric maps were combined, the best classification accuracy was obtained (86%). *CONCLUSIONS:* Textural characteristics of quantitative ultrasound spectral parametric maps provided discriminant information about different types of breast tumors. The use of texture features significantly improved the results of ultrasonic tumor characterization compared to conventional mean values. Thus, this study suggests that texture-based quantitative ultrasound analysis of *in vivo* breast tumors can provide complementary diagnostic information about tumor histologic characteristics.

Translational Oncology (2014) 7, 759–767

Introduction

Breast cancer is the most frequently diagnosed cancer in women, excluding skin cancer, and the second most common cause of cancer related death in women [1]. In the United States, breast cancer affects one in eight women over the course of their lifetime [2]. Breast cancers range from small early-stage tumors to larger locally advanced cancers. Early stage breast tumors tend to be less than 2 cm in size and low in histologic grade. Locally advanced breast cancer (LABC), on the other hand, is an aggressive subtype of breast cancer (mainly stage III) that is clinically characterized as being larger than 5 cm, often unresectable, and with chest wall, ipsilateral supraclavicular, infraclavicular, skin, or lymph node involvement. Despite treatment efforts using systemic chemotherapy, surgery, and radiation therapy,

Address all correspondence to: Dr. Gregory J. Czarnota, Departments of Radiation Oncology, and Imaging Research, Sunnybrook Health Sciences Centre, and Sunnybrook Research Institute, 2075 Bayview Avenue, T2-185, Toronto, Ontario, M4N 3M5.
E-mail: Gregory.Czarnota@sunnybrook.ca
Received 25 July 2014; Revised 15 October 2014; Accepted 17 October 2014

1936-5233/14
http://dx.doi.org/10.1016/j.tranon.2014.10.007

estimated 3- and 5-year survival rates of 70% and 55% were reported, respectively, in the United States in 2004 for women with stage III breast cancer [3]. LABC outcomes are typically worse, with 5-year survival rates less than 50% [4].

An accurate diagnosis of breast tumors plays an important role in prognosis and therapy planning, and can improve overall survival. X-ray mammography is currently the primary imaging modality for breast examinations. However, mammographic sensitivity declines significantly with increasing breast density particularly in young women [5]. Clinical ultrasound, when performed in conjunction with mammography, has been reported to increase diagnostic accuracy (area under the receiver-operator characteristic [ROC] curve) from 0.78 to 0.91 [6]. However, due to the many instrument parameters that can be chosen during an ultrasound imaging session, a comparative interpretation of conventional B-mode images becomes difficult when different imaging settings are applied or when different ultrasound machines are used. In addition, B-mode images, which are used by radiologists for breast examination, lack readily accessible information about microstructural properties of soft tissues. This information is lost when raw ultrasound data, or radiofrequency (RF) data, are converted to gray-scale pixels. Quantitative ultrasound (QUS) techniques, which examine the frequency dependence of backscatter from tissues (from analyzed RF data), have been developed to overcome these limitations. Such techniques have been applied *in vivo* in a variety of applications to reveal information about tissue microstructure, enabling the differentiation of disease from nondisease and the characterization of disease into its subtypes. Applications include the characterization of tissue abnormalities, such as those in the eye, prostate, and myocardium, and to detect and classify cancer in the lymph nodes [7–10]. Specifically, QUS parameters including average scatterer diameter (ASD) and average acoustic concentration (AAC; related to effective scatterer number density and relative acoustic impedance) have demonstrated the potential to be used to distinguish between mouse models of mammary carcinoma and rat models of fibroadenoma. These parameters can be obtained by fitting a form factor model, such as the Gaussian form factor, to the measured backscatter coefficient [11–13]. To avoid complex model fitting, basic spectral parameters extracted via a linear regression analysis of the RF power spectrum, including mid-band fit (MBF), spectral slope (SS), and spectral 0-MHz intercept (SI), have also been used for tissue characterization previously [7–10]. By modeling the ultrasonic power spectrum as an acoustic impedance autocorrelation function, Lizzi et al. demonstrated that parameters, extracted from a linear fit to the power spectrum within the usable frequency bandwidth, are related to the scattering properties of the tissue of interest. In particular, they found that SS is related to effective scatterer size and attenuation, SI is related to effective scatterer size and acoustic concentration, and MBF is related to effective scatterer size, acoustic concentration, and attenuation [14,15]. As frequency-dependent backscatter measurements are affected by the inherent frequency-dependent attenuation of intervening tissues, it is standard to compensate the tissue power spectrum for frequency-dependent attenuation before computing spectral parameters, as done in many studies [8–10].

Frequency-dependent attenuation has also been shown to be a useful parameter in characterizing tissues, especially tumors and normal tissues of the breast [16]. Furthermore, a previous clinical study found large variations in the attenuation coefficient estimates (ACEs) among breast carcinoma tumors (1.16±0.8 dB/cm per MHz), which included invasive ductal carcinoma, invasive lobular carcinoma, intracystic papillary carcinoma, and adenocarcinoma [17]. Another parameter, scatterer spacing, also known as spacing among scatterers (SAS), has been investigated as a tissue characterization parameter when the tissue of interest contains detectable periodicity in its structural organization. Previous studies have investigated the potential of SAS mainly for characterizing diffuse diseases of the liver [18,19]. For instance, in [20], the interscatterer distribution and the mean scatterer spacing (MSS) were examined in focal diseases of the liver using wavelet transform–based methods, whereas in [21], the MSS was considered for characterization of pathologic human liver using Fourier transform–based methods. The terms *SAS* and *MSS* are used interchangeably in the literature to refer to the mean scatterer spacing in a scattering volume. More recently, SAS was used to characterize human breast tumors in terms of normal breast tissue, fibroadenoma, simple carcinoma, and infiltrating papillary carcinoma [22]. SAS was determined to be 1.25 ± 0.21 μm for normal breast tissue, 0.82 ± 0.10 μm for simple carcinoma, 0.92 ± 0.09 μm for infiltrating apillary carcinoma, and 1.09 ± 0.07 μm for breast adenoma; however, no statistical significance tests comparing these tissue abnormalities were reported.

Whereas the conventional quantitative ultrasound spectral parameters discussed above describe the frequency-dependent properties of tissue microstructure, an analysis of textural characteristics of QUS-based parametric maps can potentially provide second-order statistics by quantifying the patterns of gray-level transitions. In 1983, Wagner et al. demonstrated that the second-order statistical properties (based on the Rayleigh distribution) of B-mode images carry subresolution information about the medium's microstructure [23]. Following this work, various statistical models were developed to further characterize the textural properties of B-mode images [24,25]. Alternatively, second-order textural properties of images, including but not limited to ultrasound, can be quantified using the gray-level co-occurrence matrix (GLCM). Initially developed as an image classification tool for landmark aerial photographs and sandstone photomicrographs [26], the application of the GLCM was later extended to ultrasound tissue characterization, such as discriminating between benign and malignant breast tumors [27,28]. The principle behind this tissue classification technique is that malignant tumors tend to present as heterogeneous internal echoes, whereas benign masses often demonstrate homogeneous internal echoes. Textural analysis techniques aim at extracting the tissue internal echo properties or "texture," based on the ultrasonic gray-level transitions, and hence can define differentiable characteristics in this application. However, previous studies [27,28] have used conventional B-mode images for textural analysis, which may present undesirable variations in textural estimates due to variations in instruments settings, ultrasound beam diffraction, and attenuation effects. Such limitations can be addressed by performing texture analysis on quantitative ultrasound parametric images for which these artifacts have been compensated. In a study by Sadeghi-Naini et al. [29], texture analysis based on a GLCM was applied to ultrasonic parametric maps (i.e., MBF, SS, and SI) to characterize tumor cell death responses to chemotherapy *in vivo*. Extracted GLCM features were contrast, energy, and homogeneity. In a study by Tadayyon et al. [30], a similar texture analysis was applied to ASD, AAC, and SAS images of LABC tumors in addition to MBF, SS, and SI images for purposes of tumor grade discrimination. Here, we examined the means and four GLCM features (contrast, correlation, energy, and homogeneity) of six QUS parameters, as done in [30], for

characterization of LABC tumors. However, new in this study, all QUS parametric maps were obtained after spectral attenuation correction using the ACE values obtained via the spectral difference method, and the ACE parameter was also included in the discriminant analysis. Furthermore, leave-one-patient-out training and testing were performed for tumor grade classification, which were not done in previous studies. Results here suggest that large tumors can be graded with 82% accuracy using textural features of spectral parametric maps, and a further classification accuracy of 88% can be obtained using the combination of means of the parametric maps and textural features.

Materials and Methods

The breast tissue characterization technique used here was a two-stage process involving QUS parameter estimation followed by classification. Given a tumor region of interest (ROI) in a breast ultrasound image, QUS parameters including MBF, SS, SI, SAS, ASD, AAC, and ACE were computed from its RF data. In addition to the mean, textural features including contrast, correlation, energy, and homogeneity were determined from the parametric map based on a GLCM [26].

A total of 31 features were considered for characterization: means from six parametric maps (MBF, SS, SI, SAS, ASD, AAC), a single-value parameter (ACE), and four texture features per parametric map ($4 \times 6 = 24$ texture features in total). The Fisher linear discriminant was used to classify tissues using different QUS feature combinations [31]. The goal of Fisher linear discriminant is to project the data onto a feature space which maximizes the ratio of the between-class variance to within-class variance. The threshold was chosen as the hyperplane between the means of the projected data. Finally, a leave-one-out analysis was performed on the classification of grade I versus grade II to III tumors and metrics such as grade I prediction rate, grade II to III prediction rate, accuracy, and area under the ROC curve were used to evaluate the classification results. The rationale for separating grade I tumors from grade II and III tumors was that patients with grade I tumors are low-risk patients compared to patients with grade II and III tumors in terms of their management.

Ultrasound data acquisition and processing

LABC patients ($N = 57$, N G1 = 7, N GII to III = 50) were recruited in this study for noninvasive tumor grading (Table 1). The study followed a protocol approved by the institution's research ethics board from Sunnybrook Health Sciences Centre, Toronto, ON, Canada. Signed consent was obtained from all patients before the scans. Patients with large tumors (3 cm or larger) were selected in this study to avoid uncertainties in tumor identification. All information regarding histopathologic characteristics of the tumors, including type and grade, were determined from clinical biopsy pathology reports before the imaging session. In a clinical context, this QUS assessment of the breast can be performed during an ultrasound-guided biopsy session or after a biopsy session to cross-verify the tumor grade found from the biopsy sample examination. Tumor size was defined as the sum of the long axis lengths of the tumor foci and was determined from diagnostic magnetic resonance imaging reports. For performing supervised learning using linear discriminant analysis, tumors were histologically divided into two classes: grade I and grade II to III. This used the maximum number of available tumors in the study because roughly 30% of the tumors were identified by institutional pathologists as intermediate-to-high grade rather than a definitive grade II or grade III. RF and B-mode ultrasound data were collected from the affected breast using a Sonix RP ultrasound scanner operating a 6-MHz–stimulated broadband array transducer (L14-5/38, Ultrasonix, Vancouver, Canada). RF data were sampled at 40 MHz at a 512-line density, resulting typically in images with 6-cm width and 4- to 6-cm depth. Four to seven image planes of the tumor were selected at 1-cm intervals across the affected breast for analysis.

Table 1. Summary of Patient Demographics and Clinical Tumor Characteristics

Characteristic	Total ($N = 57$)	
	No.	%
Age (y)	49 (29-67)	
Tumor size (cm)	6.5 (1.9-15)	
Tumor subtype		
IDC	53	93
ILC	1	1.8
IDC (mucinous features)	1	1.8
IDC (basal-like)	1	1.8
Metaplastic carcinoma	1	1.8
GI	7	12
GII to III	50	88

Abbreviations: IDC = invasive ductal carcinoma, ILC = invasive lobular carcinoma.

An oncologist was present at the baseline (pretreatment) imaging session to locate the tumor and its extent in the ultrasound navigation. ROIs enclosing the central mass of the tumor (approximately 90% of tumor volume) were selected across four to seven tumor cross-sections under the guidance of an oncologist. The ROIs were selected manually from B-mode images using an in-house MATLAB image segmentation program by one user (H.T.) and verified by the oncologist. The margins of the tumor were excluded to avoid any ambiguities in the boundary definitions. Each ROI was then segmented using a sliding window approach with 80% overlap between adjacent windows. Each window had dimensions of 2 mm by 2 mm. The size of the window was selected to cover approximately 17 ultrasound wavelengths, larger than the minimum size (10 wavelengths) typically required to obtain reliable spectral slope estimates which are independent of window length [32].

To make the analysis method system independent, processed ultrasound data were normalized on a sliding-window basis using reference data obtained from a tissue-mimicking phantom or a planar reflector. For linear regression analysis of the power spectrum, an in-house–constructed tissue-mimicking phantom was used, comprising of agar gel embedded with glass microspheres (modified from [33]). For SAS analysis, a Plexiglas planar reflector was used as reference, as SAS estimation is sensitive to the spatial distribution of the scatterers in the reference medium, and a planar reflector has relatively simpler scattering properties compared to those of the phantom used in this study. Echo data from the polished Plexiglas surface were obtained at 12 equally spaced depths from 1 to 6 cm, which covered all possible breast tumor depths. For a given tumor window, the corresponding reference window was selected by nearest neighbor interpolation. The data normalization process is discussed in more detail below.

Quantitative Ultrasound Spectral Analysis

All spectral analyses were carried out using the −6-dB system transducer bandwidth, which was 3 to 8 MHz. The first step in the QUS analysis was computation of the ACE of the tumor, which was required for attenuation correction of the tumor power spectrum. The ACE was computed using the spectral difference method by estimating the rate of change in the spectral magnitude with depth

and frequency relative to a reference medium with a known attenuation coefficient [34]. The reference medium was a well-characterized tissue-mimicking phantom with known attenuation coefficient (0.15 dB/cm per MHz) and speed of sound (1539 m/s). Plots of relative spectral amplitude versus depth were obtained by averaging the normalized window power spectra across laterally adjacent windows and then plotting the average amplitude at each frequency against the depth of the windows in the ROI. The ACE of the tumor was estimated by averaging the slopes of the linear fits to the amplitude versus depth data at all frequency points in the bandwidth. An attenuation coefficient of 1 dB/cm per MHz was assumed for intervening breast tissue based on ultrasound tomography measurements of the breast [35]. A two-layer (intervening tissue and tumor) attenuation correction was performed using total attenuation estimation (Equation (2), Ref. [34]) and point attenuation compensation method [36]. Afterwards, spectral parameters, including MBF, SI, and SS, were extracted from linear regression of the attenuation-corrected power spectrum within the −6-dB bandwidth using established spectral analysis methods [14]. MBF was defined as the value of the spectral linear fit at the center of the analysis bandwidth (i.e., 5.5 MHz).

Using the same attenuation-corrected power spectrum, the backscatter coefficient (BSC) of the tumor was estimated using the reference phantom technique [37]. Then, by least squares fitting of the Gaussian form factor to the BSC, parameters of the Gaussian form factor, ASD and AAC, corresponding to the maximum coefficient of determination, 2, were determined. Details about scatterer size estimation can be found elsewhere [38].

Whereas spectral linear regression and BSC models are based on incoherent scattering, cepstral analysis techniques allow coherent scattering properties of tissues to be derived [39]. In this light, the power spectrum of the tumor was determined by modeling the tumor echo signal as an autoregressive signal and using Burg's algorithm to estimate its power spectrum. The power spectrum was then normalized to that of a planar reflector. By computing the autocorrelation of the normalized power spectrum, the SAS parameter was determined from the frequency at which the peak occurred in the autocorrelation [19]. SAS estimation requires one to know the speed of sound in the ROI. For tumor ROIs in this study, a sound speed of 1540 m/s was assumed. These values are consistent with ultrasound tomography–derived measurements of speed of sound in the breast [40].

Statistical Textural Analysis of Quantitative Ultrasound Maps

In this study, a statistical texture analysis technique was applied that is based on the concept of GLCM. The GLCM represents, statistically, the angular relationship between neighboring pixels as well as the distance between them [26]. Based on the statistical information provided by GLCM analysis, several textural features were determined including contrast (CON), correlation (COR), homogeneity (HOM), and energy (ENE), as defined in Equations (1–4).

Parametric maps of MBF, SS, SI, SAS, ASD, and AAC each underwent a GLCM-based texture analysis process to extract four textural features. Texture properties could not be extracted from ACE because a single value was computed from each ROI rather than computing a parametric map, as a large number of points (depths) were required to obtain accurate estimates of attenuation slope. In texture analysis, the contrast feature represents a measure of difference between the lowest and highest intensities in a set of pixels. The energy feature measures the frequency of occurrence of pixel pairs and quantifies its power (square of the frequency of gray-level transitions). The homogeneity feature measures the incidence of pixel pairs of different intensities. As the frequency of pixel pairs with close intensities increases, homogeneity increases. The correlation feature measures the correlation between pixel pairs. Given $\rho(i,j)$, an element in a $Ng \times Ng$ GLCM, where $Ng = 8$ is the number of gray levels, the textural features were defined as follows [26,28]:

$$CON = \sum_{i-j=0}^{N_g-1} (i-j)^2 \sum_{i=1}^{N_g} \sum_{j=1}^{N_g} p(i,j) \tag{1}$$

$$ENE = \sum_{i=1}^{N_g} \sum_{j=1}^{N_g} p(i,j)^2 \tag{2}$$

$$HOM = \sum_{i=1}^{N_g} \sum_{j=1}^{N_g} \frac{p(i,j)}{1+|i-j|} \tag{3}$$

$$COR = \frac{\sum_{i=1}^{N_g} \sum_{j=1}^{N_g} (i-\mu_i)(j-\mu_j) p(i,j)}{\sigma_i \sigma_j} \tag{4}$$

where μi, σi are the mean and standard deviation of the ith row of the GLCM and μj, σj are the mean and standard deviation of the jth column of the GLCM. Sixteen symmetric GLCMs were constructed for each parametric map, corresponding to four pixel-to-pixel distances (1 pixel, 2 pixels, 3 pixels, and 4 pixels) and four directions (0°, 45°, 90°, and 135°). The texture feature for each of the 16 symmetric GLCMs was computed and averaged to obtain a mean texture value. This resulted in 24 mean textural features (four features for each of the six parametric maps) that were subsequently applied for characterizing tumors in terms of their grade.

Tumor Grade Classification

Sequential feature selection [41, Table 5] was performed for 3 cases: 7 QUS means (MBF, SS, SI, SAS, ACE, ASD, AAC), 24 texture features, and 31 means and texture features combined. The first step of the sequential feature selection involved performing unpaired t tests on all individual features to compare their group means (all features were found to be normally distributed based on the Shapiro-Wilk normality test). The features were then sorted from lowest to highest P value. Starting with the lowest P value feature as the initial model, features were sequentially added to or discarded from the model until there was no improvement in classification. The features of the final model resulting from the sequential feature selection were termed the *optimal features*.

A leave-one-patient-out analysis was performed on $N = 57$ patients using QUS features obtained by averaging across the tumor cross sections to obtain a volumetric average for each patient. The true labels (tumor grade) were determined from biopsy findings. For each patient left out, the $N - 1$ patients were used to train the classifier, and the remaining one patient was used to predict its response. The process was repeated N times to obtain classifier predictions from all N tested patients.

Table 2. Summary of Classification Performances for Optimal Features Obtained from Sequential Feature Selection from All Means, All Textures, and All Means and Textures

	GI Prediction Rate (%)	GII to III Prediction Rate (%)	Overall Accuracy (%)	A_Z (LB, UB)
Optimal means	57	82	79	0.71(0.49, 0.94)
Optimal textures	43	88	82	0.74 (0.52, 0.96)
Optimal means and textures	**71**	**88**	**86**	**0.76 (0.54, 0.97)**

All results were obtained by leave-one-out cross-validation. A_Z is the area under the ROC curve, LB and UB are the lower and upper 95% confidence bounds of A_Z.

Results

Patient Characteristics

Relevant patient characteristics, including age, tumor size, tumor type, and tumor grade, are listed in Table 1. Patients were aged between 29 and 67 and had a mean tumor size of 6.5 cm (range, 1.9 to 15 cm). Tumors were predominantly of the invasive ductal carcinoma type (91%), with the exception of one case of invasive ductal carcinoma with mucinous features, one case of invasive ductal carcinoma with basal-like features, one case of invasive lobular carcinoma, and one case of metaplastic carcinoma. The tumors were largely grade II to III ($N = 50$), with a few incidences of grade I tumors ($N = 7$), determined by institutional pathologists from surgical biopsy specimens.

Quantitative Ultrasound

Linear discriminant analysis results obtained from three cases: using the means of all parametric maps, using the texture features of all parametric maps, and using both the means and textures of all parametric maps, are summarized in Table 2. GI prediction rate was defined as the percent ratio of correctly classified GI samples to all GI samples, and GII to III prediction rate was defined as the ratio of correctly classified GII to III samples to all GII to III samples. Accuracy was defined as the ratio of all correctly classified samples to all samples. All results were obtained after leave-one-out cross-validation. The results demonstrated that using only the means of the parametric maps yields lower accuracy (79%) compared to using the textural features (82%). Furthermore, combining means and textural features further improved the accuracy of the classification (86%). In all cases, lower GI prediction rate was obtained compared to GII to III prediction rate.

Table 3 presents the structure vector, which consists of the optimal features obtained from sequential feature selection from all QUS means and textures and their coefficients. The linear discriminant function was composed of 18 features. The shown coefficients represent the correlation between each feature and the obtained discriminant function. A higher absolute value indicates a higher relevance of the feature to the discrimination of the classes. It is evident from Table 3 that the COR feature was the most frequently appearing feature with relatively strong contribution to the discriminant function, as it appeared for SAS ($R^2 = 0.213$), SS ($R^2 = 0.194$), and AAC ($R^2 = 0.179$). Another observation was that all SAS texture features and means proved to contribute to the discrimination of tumor grades, indicating that SAS played an important role in the tumor grade classification.

ROC curves for the three cases, obtained from the cross-validated data set, are presented in Figure 1. The ROC curve approaches the optimal point (upper left corner) as better feature sets are selected (means, textures, and combined means/textures, respectively).

Table 3. Discriminant Function Structure Vector for Optimal QUS Means and Textures

Rank	Feature	Coefficient
1	SAS_{ENE}	0.236
2	SAS_{COR}	0.213
3	SS_{COR}	0.194
4	AAC_{COR}	0.179
5	SI_{HOM}	0.143
6	AAC_{mean}	−0.131
7	ASD_{HOM}	0.126
8	SAS_{HOM}	−0.116
9	AAC_{ENE}	0.098
10	ACE_{mean}	0.093
11	ASD_{ENE}	−0.086
12	SAS_{mean}	−0.069
13	AAC_{HOM}	0.061
14	SAS_{CON}	0.057
15	SS_{ENE}	0.048
16	MBF_{ENE}	−0.048
17	SS_{CON}	−0.046
18	SI_{CON}	−0.038

Coefficients represent the correlation between each feature and the obtained discriminant function. Features are listed in order of decreasing absolute coefficient.

Based on the classification results, a hybrid parameter was determined that represents the linear combination of a subset of QUS means and textures that provides the optimal classification accuracy (row 3 of Table 2). This parameter is equivalent to the output of the optimal linear discriminant function whose structure vector is provided in Table 3. Figure 2 presents a one-dimensional scatter plot of the hybrid parameter values for all patients grouped in terms of their tumor grade. The linear discriminant function was optimized to produce positive values for grade I tumors and negative values for grade II to III tumors. The difference between the mean hybrid values of grade I and grade II to III tumors was determined to be statistically significant ($P < .05$).

Figure 3 shows representative B-mode images, hybrid parameter images, and hematoxylin and eosin histology sections of grade I, II, and III tumors. For QUS means, QUS window values were used to compute the linear discriminant function in each window. For QUS textures, all windows were assigned a constant texture value for each texture feature (CON, COR, ENE, HOM) because the GLCM was computed from the ROI rather than the window. Because QUS means have a lower weight in the discriminant function compared to texture features, the resulting parametric image will have relatively small standard deviation, as can be seen in Figure 3*B*. Figure 3*B* presents the hybrid image in a common scale to help realize the differences between the tumors, whereas Figure 3*C* presents the hybrid images in individually optimized scales to help visualize the internal deviations. Whereas the conventional B-mode images presented all breast tumors as complex hypoechoic masses with little differences in terms of grade and difficult-to-visualize features, the hybrid images demonstrated a clear trend of decreasing hybrid value with increasing tumor grade. Histology images show cancerous glands as purple-stained structures, the stroma as pink-stained structures, and adipose tissue as white structures. The images depict cancerous tissue with increasingly disordered clusters of cancerous glands and decreasing stromal density with increasing grade.

Discussion

This study demonstrated for the first time the efficacy of textural analysis techniques on QUS parametric maps to discriminate between grade I and grade II to III breast tumors. After acquiring several planes

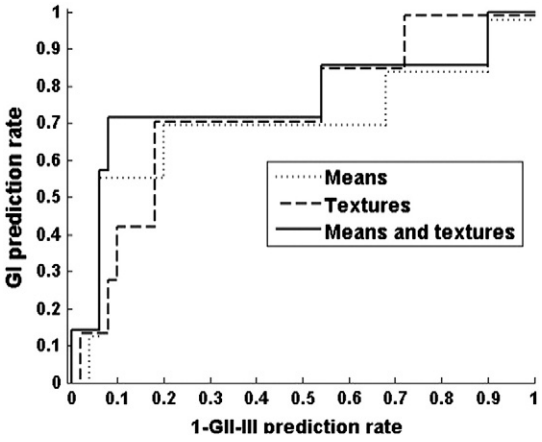

Figure 1. ROC curves for the different feature sets. Set *A*: means and textures of MBF, SS, SI, and SAS, plus ACE. Set *B*: means and textures of ASD, AAC, and SAS, plus ACE. Set C, all parameter means and textures included.

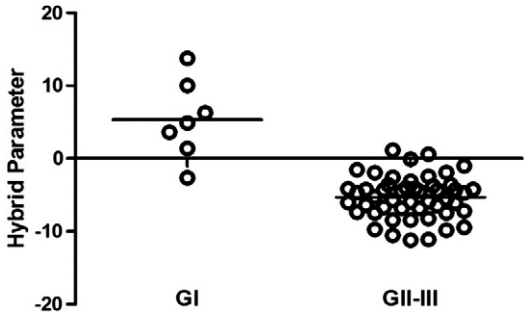

Figure 2. One-dimensional scatter plot of the hybrid QUS biomarker versus tumor aggressiveness. Each point represents the hybrid QUS value of each patient. The horizontal lines represent the means of the groups.

of RF data from tumors of patients with LABC, features such as mean, CON, COR, ENE, and HOM were extracted from QUS parametric maps computed from tumor ROIs within the breast. An optimal feature set was selected using sequential feature selection, and linear discriminant analysis was performed on the set with cross-validation using true labels identified histopathologically from biopsy specimens. Three types of feature sets were considered: feature selection from means, textures, and the combinations of means and textures. The most accurate classification was obtained when the combination of QUS means and textures was used (86% accuracy).

Quantitative ultrasound has been investigated in the past as an aid to characterize breast tumors *in vivo* and to differentiate clinically malignant breast tumors from benign masses [22,28,42,43]. Specifically, the work of Oelze et al. [42] has demonstrated the ability to differentiate mouse mammary carcinoma from benign rat fibroadenomas using mean values of scatterer size and acoustic concentration parametric maps obtained from a 20-MHz ultrasound system. On the other hand here, the differentiation between lower-grade tumors (analogous to benign fibroadenomas) and mid- to high-grade tumors (analogous to mammary carcinoma) was best seen using the textural features of acoustic concentration (AAC) and scatterer size (ASD), giving accuracy as high as 86%. Mean values yielded less than optimal separation (79 %). Similarly, when Nasief et al. [43] investigated QUS features such as scatterer size, attenuation, and heterogeneity index to differentiate clinically benign breast tumors from malignant ones, only subtle differences could be found because only mean values were considered. The parametric images here (Figure 3), however, suggested clear distinctions between tumors of different grades when textures of QUS parameters were included.

Similar to the finding in our previous study that the linear combination of ASD mean and texture features demonstrated a better separation between tumor grades than did ASD mean or textures alone [30], the linear combination of QUS parameter means and texture features demonstrated better classification results than did means or texture features alone. Our previous study [30] lacked attenuation correction of spectra using tumor-specific attenuation coefficient estimates and reported statistical significances of QUS differences between tumor grades; no tumor grade classification was performed. Here, we have included tumor-specific attenuation correction and have performed linear discriminant analysis including leave-one-out classifier evaluation. It should be noted that other attenuation correction functions are available, which take into account the gate length, such as Oelze and O'Brien and O'Donnell and Miller methods [36]. However, these functions offer accuracy advantages only for large gate lengths. For the relatively small gate length used in this study (2 mm), the point-attenuation, Oelze and O'Brien, and O'Donnell and Miller methods all result in similar scatterer size estimations, as demonstrated in [36], Figure 5.

In this study, texture analysis of the QUS parametric maps of different grades of breast tumors demonstrated an 82% classification accuracy when the texture features of QUS parametric maps were used (CON, COR, ENE, HOM), whereas using only means resulted in a classification accuracy of 79%. A further improvement in classification was achieved when the means of parametric maps were combined with the textures (86% accuracy).

Interuser variability should be minimal, although in this study, only one user selected ROIs consistently, which were checked by one oncologist. One of the limitations of this technique was tumor size (>3 cm). As QUS textural features are sensitive to heterogeneity of the tumor, the tumors must be sufficiently large to be differentiable in terms of their internal ultrasonic echo properties. Smaller tumors may limit outcomes of this work. There is also an issue of variability in QUS feature estimates due to the user dependence of the manual segmentation process involved. However, variability in QUS feature estimates due to different ROI locations was minimized by consistently imaging each tumor in the focal region of the transducer, thereby avoiding regions of near field, far field, and diffraction. It is acknowledged that relatively lower GI prediction rates were obtained compared to GII to III prediction rates. This is likely due to the presence of imbalanced data, where there are much more grade II to III cases than grade I cases, naturally driving the classifier to learn the data pattern of the more populated group more effectively. Compensation for imbalanced data sets is an active area of research and requires thorough investigation in a separate study. Nevertheless a leave-one-out analysis here was able to fairly accurately identify grade I tumors compared to grade II to III tumors, which are often managed differently in terms of clinical care. The complexity of the proposed model is acknowledged given the large number of features compared to the number of observations. However, the effects of overfitting were minimized by performing sequential feature selection

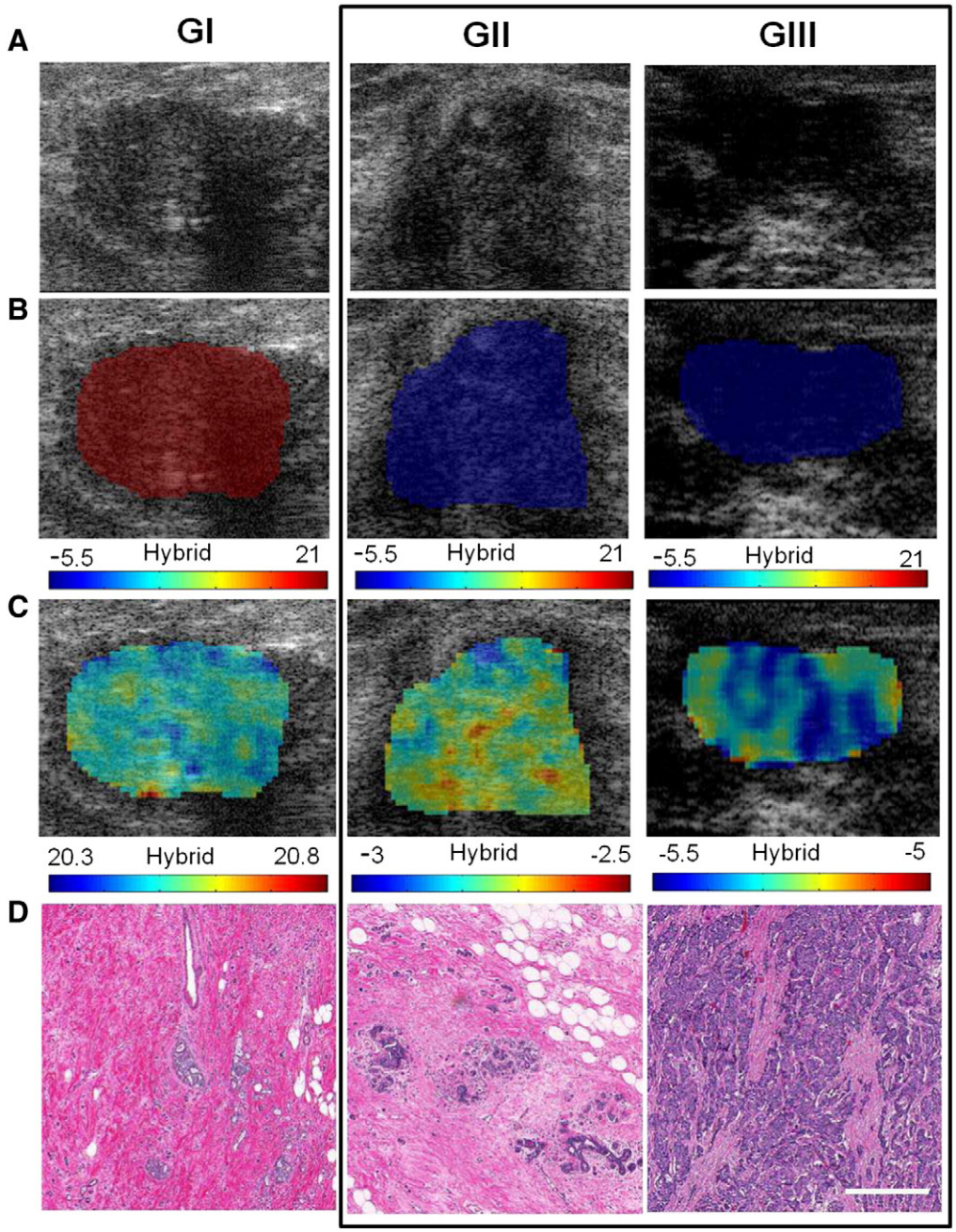

Figure 3. Representative images of grade I, II, and III breast tumors. (A) B-mode images of the tumor regions, where the tumors appear as hypoechoic masses. (B) Corresponding hybrid QUS biomarker images of the tumors obtained from optimized linear combination of original QUS means and textures. A common scale bar was used to include the range for all three tumors. (C) Corresponding hybrid QUS biomarker images of the tumors obtained from optimized linear combination of original QUS means and textures. Individual scale bars were used to show the standard deviations in each tumor. (D) Hematoxylin and eosin–stained histopathology images of the tumors. Scale bars: 1 cm (US), 100 μm (hist).

to find the minimum number of features (18 features) that can provide optimal classification accuracy, excluding noncontributing or minimally contributing features. Additionally, the leave-one-patient-out analysis performed has been known to minimize overfitting [44].

As previously mentioned, acoustic concentration is the product of scatterer number density and acoustic impedance difference between the scatterer and the background, and acoustic impedance is the product of sound speed and density. Thus, the fact that parameters related to the scatterer spacing and acoustic concentration including SAS, AAC, MBF, and SI formed the major portion of the discriminant function (Table 2) compared to parameters related to the scatterer size (i.e., SS and ASD) suggests that the spatial organization and material properties of the tumor microstructure play a more important role than its size in the discrimination of tumor histologic grades. This was not surprising because the breast tumor is a complex tissue containing blood vessels, adipose tissue, and stroma, in addition to cancerous glands. Thus, scatterer size may not refer to the size of glands alone but to a mixture of structures.

In summary, breast tumor grading is an important part of breast cancer diagnosis and provides valuable information for treatment planning. In this light, noninvasive methods such as texture-based QUS analysis can provide beneficial diagnostic information that can be applied before and during the course of treatment. This study demonstrated a high potential for textural characteristics of QUS parametric maps to be used in the diagnosis and grading of breast tumors. The best tissue classification could be achieved when the combination of mean and textural properties of MBF, SS, SI, SAS, ASD, and AAC parametric maps was used. This work provides a framework for future clinical studies in which the proposed classification scheme is evaluated on larger cohorts of patients to further assess its capabilities for an accurate breast tumor diagnosis and grading noninvasively.

Acknowledgments

A.S.N holds a Banting Postdoctoral Fellowship. G.J.C. holds a Cancer Care Ontario Research Chair in experimental therapeutics and imaging. This study was funded, in part, by the Canadian Breast Cancer Foundation - Ontario Region. Funding for this project was also provided by the Terry Fox Foundation, Natural Sciences and Engineering Research Council of Canada and Canadian Institutes of Health Research.

References

[1] American Cancer Society (2013). Cancer Facts and Figures 2013; 2013 [Atlanta].

[2] U.S. Breast Cancer Statistics (2013). [Online]. Available http://www.breastcancer.org/symptoms/understand_bc/statistics.jsp; 2013.

[3] Giordano SH (2003). Update on locally advanced breast cancer. *Oncologist* **8**(6), 521–530.

[4] Yalcin B (2013). Overview on locally advanced breast cancer: defining, epidemiology, and overview on neoadjuvant therapy. *Exp Oncol* **35**(4), 250–252.

[5] Kolb TM, Lichy J, and Newhouse JH (2002). Comparison of the performance of screening mammography, physical examination, and breast US and evaluation of factors that influence them: an analysis of 27,825 patient evaluations. *Radiology* **225**(1), 165–175.

[6] Berg WA, Blume JD, Cormack JB, Mendelson EB, Lehrer D, Böhm-Vélez M, Pisano ED, Jong RA, Evans WP, and Morton MJ, et al (2008). Combined screening with ultrasound and mammography vs mammography alone in women at elevated risk of breast cancer: results of the first-year screen in ACRIN 6666. *JAMA* **299**(18), 2151–2163.

[7] Coleman DJ, Lizzi FL, Silverman RH, Helson L, Torpey JH, and Rondeau MJ (1985). A model for acoustic characterization of intraocular tumors. *Invest Ophthalmol Vis Sci* **26**(4), 545–550.

[8] Feleppa EJ, Kalisz A, Sokil-Melgar JB, Lizzi FL, Liu T, Rosado AL, Shao MC, Fair WR, Wang Y, and Cookson MS, et al (1996). Typing of prostate tissue by ultrasonic spectrum analysis. *IEEE Trans Ultrason Ferroelectr Freq Control* **43**(4), 609–619.

[9] Yang M, Krueger TM, Miller JG, and Holland MR (2007). Characterization of anisotropic myocardial backscatter using spectral slope, intercept and midband fit parameters. *Ultrason Imaging* **29**(2), 122–134.

[10] Mamou J, Coron A, Oelze ML, Saegusa-Beecroft E, Hata M, Lee P, Machi J, Yanagihara E, Laugier P, and Feleppa EJ (2011). Three-dimensional high-frequency backscatter and envelope quantification of cancerous human lymph nodes. *Ultrasound Med Biol* **37**(3), 345–357.

[11] Insana MF, Wagner RF, Brown DG, and Hall TJ (1990). Describing small-scale structure in random media using pulse-echo ultrasound. *J Acoust Soc Am* **87**(1), 179–192.

[12] Mamou J, Coron A, Hata M, Machi J, Yanagihara E, Laugier P, and Feleppa EJ (2010). Three-dimensional high-frequency characterization of cancerous lymph nodes. *Ultrasound Med Biol* **36**(3), 361–375.

[13] Oelze ML, Zachary JF, and O'Brien Jr WD (2002). Characterization of tissue microstructure using ultrasonic backscatter: theory and technique for optimization using a Gaussian form factor. *J Acoust Soc Am* **112**(3 Pt 1), 1202–1211.

[14] Lizzi FL, King DL, Rorke MC, Hui J, Ostromogilsky M, Yaremko MM, Feleppa EJ, and Wai P (1988). Comparison of theoretical scattering results and ultrasonic data from clinical liver examinations. *Ultrasound Med Biol* **14**(5), 377–385.

[15] Lizzi FL, Astor M, Liu T, Deng C, Coleman DJ, and Silverman RH (1997). Ultrasonic spectrum analysis for tissue assays and therapy evaluation. *Int J Imaging Syst Technol* **8**(1), 3–10.

[16] D'Astous FT and Foster FS (1986). Frequency dependence of ultrasound attenuation and backscatter in breast tissue. *Ultrasound Med Biol* **12**(10), 795–808.

[17] Nam K, Zagzebski JA, and Hall TJ (2013). Quantitative assessment of in vivo breast masses using ultrasound attenuation and backscatter. *Ultrason Imaging* **35**(2), 146–161.

[18] Suzuki K, Hayashi N, Sasaki Y, Kono M, Kasahara A, Imai Y, Fusamoto H, and Kamada T (1993). Evaluation of structural change in diffuse liver disease with frequency domain analysis of ultrasound. *Hepatology* **17**(6), 1041–1046.

[19] Wear KA, Wagner RF, Insana MF, and Hall TJ (1993). Application of autoregressive spectral analysis to cepstral estimation of mean scatterer spacing. *IEEE Trans Ultrason Ferroelectr Freq Control* **40**(1), 50–58.

[20] Abeyratne UR and Tang X (2007). Ultrasound scatter-spacing based diagnosis of focal diseases of the liver. *Biomed Signal Process Control* **2**(1), 9–15.

[21] Machado CB, Pereira WCA, Meziri M, and Laugier P (2006). Characterization of in vitro healthy and pathological human liver tissue periodicity using backscattered ultrasound signals. *Ultrasound Med Biol* **32**(5), 649–657.

[22] Bige Y, Hanfeng Z, and Rong W (2006). Analysis of microstructural alterations of normal and pathological breast tissue in vivo using the AR cepstrum. *Ultrasonics* **44**(2), 211–215.

[23] Wagner RF, Smith SW, Sandrik JM, and Lopez H (1983). Statistics of speckle in ultrasound B-scans. *IEEE Trans Sonics Ultrason* **30**(3), 156–163.

[24] Insana MF, Wagner RF, Garra BS, Brown DG, and Shawker TG (1986). Analysis of ultrasound image texture via generalized Rician statistics. *Opt Eng* **25**(6), 256743.

[25] Wagner RF, Insana MF, and Brown DG (1987). Statistical properties of radio-frequency and envelope-detected signals with applications to medical ultrasound. *J Opt Soc Am A* **4**(5), 910–922.

[26] Haralick RM, Shanmugam K, and Dinstein I (1973). Textural features for image classification. *IEEE Trans Syst Man Cybern* **SMC-3**(6), 610–621.

[27] Alvarenga AV, Pereira WCA, Infantosi AFC, and Azevedo CM (2007). Complexity curve and grey level co-occurrence matrix in the texture evaluation of breast tumor on ultrasound images. *Med Phys* **34**(2), 379–387.

[28] Liao Y-Y, Tsui P-H, Li C-H, Chang K-J, Kuo W-H, Chang C-C, and Yeh C-K (2011). Classification of scattering media within benign and malignant breast tumors based on ultrasound texture-feature-based and Nakagami-parameter images. *Med Phys* **38**(4), 2198–2207.

[29] Sadeghi-Naini A, Falou O, Tadayyon H, Al-Mahrouki A, Tran W, Papanicolau N, Kolios MC, and Czarnota GJ (2013). Conventional frequency ultrasonic biomarkers of cancer treatment response in vivo. *Transl Oncol* **6**(3), 234–243.

[30] Tadayyon H, Sadeghi-Naini A, Wirtzfeld L, Wright FC, and Czarnota G (2014). Quantitative ultrasound characterization of locally advanced breast cancer by estimation of its scatterer properties. *Med Phys* **41**(1), 012903.

[31] Krzanowski WJ (1988). Principles of Multivariate Analysis: A User's Perspective. New York: Oxford University Press; 1988 .

[32] Topp KA, Zachary JF, and O'Brien Jr WD (2001). Quantifying B-mode images of in vivo rat mammary tumors by the frequency dependence of backscatter. *J Ultrasound Med* **20**(6), 605–612.

[33] Madsen EL, Zagzebski JA, Banjavie RA, and Jutila RE (1978). Tissue mimicking materials for ultrasound phantoms. *Med Phys* **5**(5), 391–394.

[34] Labyed Y, Bigelow TA, and McFarlin BL (2011). Estimate of the attenuation coefficient using a clinical array transducer for the detection of cervical ripening in human pregnancy. *Ultrasonics* **51**(1), 34–39.

[35] Duric N, Littrup P, Babkin A, Chambers D, Azevedo S, Kalinin A, Pevzner R, Tokarev M, Holsapple E, and Rama O, et al (2005). Development of ultrasound tomography for breast imaging: technical assessment. *Med Phys* **32**(5), 1375.

[36] Oelze ML and O'Brien Jr WD (2002). Frequency-dependent attenuation-compensation functions for ultrasonic signals backscattered from random media. *J Acoust Soc Am* **111**(5, pt1), 2308.

[37] Yao LX, Zagzebski JA, and Madsen EL (1990). Backscatter coefficient measurements using a reference phantom to extract depth-dependent instrumentation factors. *Ultrason Imaging* **12**(1), 58–70.

[38] Insana MF and Hall TJ (1990). Parametric ultrasound imaging from backscatter coefficient measurements: image formation and interpretation. *Ultrason Imaging* **12**(4), 245–267.

[39] Fellingham LL and Sommer FG (1984). Ultrasonic characterization of tissue structure in the in vivo human liver and spleen. *IEEE Trans Sonics Ultrason* **SU-31**(4), 418–428.

[40] Li C, Duric N, Littrup P, and Huang L (2009). In vivo breast sound-speed imaging with ultrasound tomography. *Ultrasound Med Biol* **35**(10), 1615–1628.

[41] Jain A, Duin R, and Mao J (2000). Statistical pattern recognition: a review. *IEEE Trans Pattern Anal Mach Intell* **22**(1), 4–37.

[42] Oelze ML, O'Brien Jr WD, Blue JP, and Zachary JF (2004). Differentiation and characterization of rat mammary fibroadenomas and 4T1 mouse carcinomas using quantitative ultrasound imaging. *IEEE Trans Med Imaging* **23**(6), 764–771.

[43] Nasief H, Rosado-Mendez I, Zagzebski J, and Hall T (2013). Quantitative ultrasound as an aid to differentiate benign from malignant breast masses. AIUM (American Institute of Ultrasound in Medicine) Annual Convention; 2013. p. S62.

[44] Hastie T, Tibshirani R, and Friedman J (2011). The Elements of Statistical Learning: Data Mining, Inference, and Prediction. . 2nd ed.Springer; 2011 251.